BIOCHEMISTRY
including biophysical chemistry & molecular biology

Article

pubs.acs.org/biochemistry

Comparative Simulations of the Ground State and the M-Intermediate State of the Sensory Rhodopsin II–Transducer Complex with a HAMP Domain Model

Koro Nishikata,[†,§] Mitsunori Ikeguchi,[†] and Akinori Kidera*[,†,‡]

[†]Graduate School of Nanobioscience, Yokohama City University, Yokohama 230-0045, Japan

[‡]Research Program for Computational Science, RIKEN, Wako 351-0198, Japan

Supporting Information

ABSTRACT: The complex of sensory rhodopsin II (SRII) and its cognate transducer HtrII (2:2 SRII–HtrII complex) consists of a photoreceptor and its signal transducer, respectively, associated with negative phototaxis in extreme halophiles. In this study to investigate how photoexcitation in SRII affects the structures of the complex, we conducted two series of molecular dynamics simulations of the complex of SRII and truncated HtrII (residues 1–136) of *Natronomonas pharaonis* linked with a modeled HAMP domain in the lipid bilayer using the two crystal structures of the ground state and the M-intermediate state as the starting structures. The simulation results showed significant enhancements of the structural differences observed between the two crystal structures. Helix F of SRII showed an outward motion, and the C-terminal end of transmembrane domain 2 (TM2) in HtrII rotated by ∼10°. The most significant structural changes were observed in the overall orientations of the two SRII molecules, closed in the ground state and open in the M-state. This change was attributed to substantial differences in the structure of the four-helix bundle of the HtrII dimer causing the apparent rotation of TM2. These simulation results established the structural basis for the various experimental observations explaining the structural differences between the ground state and the M-intermediate state.

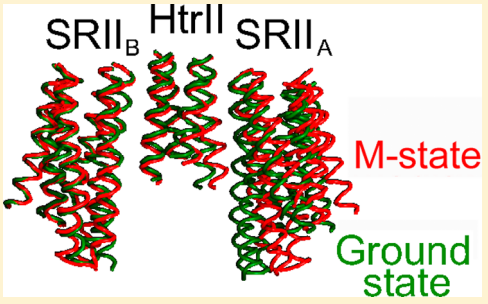

The complex of sensory rhodopsin II (SRII) and its cognate transducer HtrII [2:2 SRII–HtrII complex (Figure 1)] transfers a repellent signal for blue-green light to cytoplasmic chemotaxis proteins and finally leads to negative phototaxis.[1−4] The process of signal transduction is initiated by the photoisomerization of the retinal chromophore in SRII from all-*trans* to 13-*cis*, followed by structural changes of SRII to a series of intermediate states. These structural changes are transferred to the tightly bound transducer HtrII. Numerous studies have been devoted to resolving the mechanism of the signal transfer from retinal to SRII and then to HtrII, focusing on the difference between the ground state and the M-intermediate state of the complex of *Natronomonas pharaonis*.[5−19] In these studies, various kinds of spectroscopic techniques have been utilized: electron paramagnetic resonance (EPR) spectroscopy,[5−7] Fourier transform infrared (FTIR) spectroscopy,[8−10] solid state NMR spectroscopy,[11,12] and Förster resonance energy transfer (FRET),[13] as well as other biochemical assay techniques.[13−19] The results derived from these experiments have been mapped onto the crystal structures of the complex determined in the ground state (PDB entry 1h2s[20]).

The crystal structure of the complex determined in the late M-intermediate (PDB entry 2f95[21]) raised the possibility of resolving the signal transduction mechanism in the comparison with the ground state structure. Actually, the characteristic structural changes upon excitation that are found in EPR experiments and disulfide bond assays[5−7,14] are also observed in the M-state coordinates: the shift of helices F and G in SRII and the rotation of the C-terminal part of TM2 in HtrII (Figure 1), in addition to the local structural changes around the isomerized retinal due to the transfer of a proton from the Schiff base to D75.[22] However, the observed amplitudes of the coordinate shifts from the ground state structure are much smaller than expected in other experiments;[4,7,12] the root-mean-square deviation (rmsd) of the Cα atoms between the two crystal structures (PDB entries 1h2s and 2f95) is only 0.49 Å. It has been argued that this small change is due to the constraint originating from the crystal environment.[7] These facts give an impression that the signal transfer process has been certainly triggered, but the motions seem to be somehow stalled in the crystal environment.

In this study, we intended to remove the crystal packing effects from the crystal structures and to observe the structural differences between the ground state and the M-intermediate state in fully relaxed complex structures in a lipid bilayer using molecular dynamics (MD) simulations. Sato et al. performed MD simulations of the complex in the ground state and in K- and M-intermediate states.[23] However, because of short

Received: May 28, 2012
Revised: July 2, 2012
Published: July 3, 2012

   dx.doi.org/10.1021/bi300696b | *Biochemistry* 2012, 51, 5958−5966

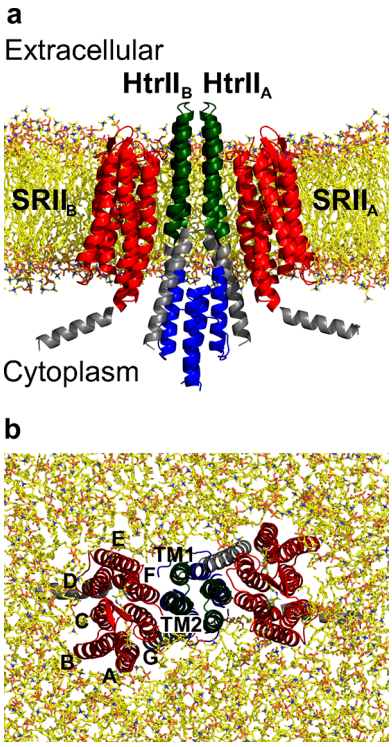

Figure 1. Simulation system of the SRII−HtrII complex with the modeled HAMP domain in a lipid bilayer. The portions of SRII and HtrII determined in the crystal structure (PDB entry 1h2s) are colored red and green, respectively. The modeled HAMP domain is colored blue, and the other modeled fragments are colored gray. The two molecules of SRII and HtrII are named SRII$_A$ and SRII$_B$, and HtrII$_A$ and HtrII$_B$, respectively, for the sake of clarity: (a) view parallel to the membrane and (b) view from the extracellular side. Molecular graphics images were generated using PyMOL (*The PyMOL Molecular Graphics System*, version 1.1r1, Schrödinger, LLC, New York).

simulation times (500 ps) and an incomplete simulation system (1:1 SRII−HtrII complex with modeled K- and M-state structures), the results were not sufficiently reliable. We have constructed simulation systems of the complex of *N. pharaonis* in the ground state and the M-intermediate state based on the two crystal structures, with all molecules in the complex (2:2 SRII−HtrII complex) appended with many missing residues [the full length of SRII (residues 1−239) and the N-terminal part of HtrII (residues 1−136), including a modeled HAMP domain (residues 84−136)] embedded in the lipid bilayer. The HAMP domain was included because of reports mentioning the importance of the interactions between the HAMP domain and SRII.[12,13,25]

MATERIALS AND METHODS

Simulation Systems. *Crystal Structures.* The simulation system, the complex of SRII (residues 1−239) and HtrII (residues 1−136), was constructed on the basis of the two crystal structures of the SRII−HtrII complex, the ground state structure (PDB entry 1h2s[20]) and the M-intermediate state structure [PDB entry 2f95 (alternate conformation B)[21]]. The missing residues were supplemented using MODELLER (version 8.2[26]) as follows. In the ground state structure, C-terminal residues 226−239 of SRII and N-terminal residues 1−22 of HtrII were appended simply by extending the α-helical structures. The method of modeling the C-terminal residues 83−136, including the HAMP domain, is explained below. In the M-intermediate state structure, residues 1, 2, and 223−239 for SRII and 1−26 and 80−136 for HtrII are appended.

Homology Modeling of the HtrII HAMP Domain. On the basis of the NMR structure of the Af1503 HAMP domain,[27] a homology model of the HtrII HAMP domain (residues 84−136) was created and equilibrated for 200 ns by molecular dynamics (MD) simulation in explicit water. The detailed methods are described in ref 28. The MD trajectory of the isolated HAMP domain was used for the model in the complex, i.e., a snapshot at 50 ns for the ground state simulation and one at 160 ns for the M-intermediate simulation. These snapshots were chosen so that the interhelical distances between the two TM2 helices matched optimally with those of the corresponding crystal structures. The two selected models have similar structures with an rmsd for the Cα atoms of 1.12 Å.

The modeled HAMP was appended as follows. After extending one residue as an α-helical structure in the ground state structure (residue 83) and four residues in the M-state structure (residues 80−83), we connected the N-terminal residue of the modeled HAMP domain (residue 84) to the C-terminal residue of the crystal structure (residue 83) while constraining the connecting region as an α-helix.

Modeling of the Complex without the HAMP Domain. As a reference to the complex with the HAMP domain, another model of the complex terminated after the first helix (called the AS1 helix) of the HAMP domain (residues 1−102) was modeled simply by extending the TM2 helix to residue 102 with MODELLER.[26]

MD Simulations of the Complex in the Lipid Bilayer. The simulation system was constructed by embedding the complex in a 1-palmitoyl-2-oleoylphosphatidylcholine (POPC) lipid bilayer in an aqueous environment. As a result, the system consisted of nearly 184000 atoms, including 440 lipid molecules and 38000 water molecules and KCl ions corresponding to 150 mM with a box size of 127 Å × 127 Å × 114 Å (Figure 1).

All the simulations were conducted with MARBLE[29] using CHARMM22[30] force fields corrected by CMAP[31] for proteins and retinal, CHARMM27[32] for lipids, and TIP3P[33] for water. Electrostatic interactions were calculated using the particle mesh Ewald method.[34] The time step was 2 fs. The Schiff base and D75 are protonated and deprotonated, respectively, in the ground state and are deprotonated and protonated, respectively, in the M-state. The entire system was equilibrated for 4.0 ns under the *NPT* ensemble (300.15 K and 1 atm) conditions with constraints against the protein and lipid non-hydrogen atoms. The constraints were gradually decreased to zero over 4 ns. Production runs were repeated twice for each state [G1, G2, M1, and M2 (Table 1)] under the *NPAT* ensemble conditions (constant surface area and constant pressure) for 100 ns without any constraints. In addition, production runs for the system without the HAMP domain were performed for each state [Gp and Mp (Table 1)] for 100 ns.

Table 1. Summary of Simulations

simulation	photochemical state of SRII	HAMP domain (the C-terminal residue of HtrII)	production run (ns)
G1, G2	ground state	−136	2 × 100
Gp	ground state	−102 (AS1 only)	100
M1, M2	M-intermediate	−136	2 × 100
Mp	M-intermediate	−102 (AS1 only)	100

dx.doi.org/10.1021/bi300696b | *Biochemistry* 2012, 51, 5958−5966

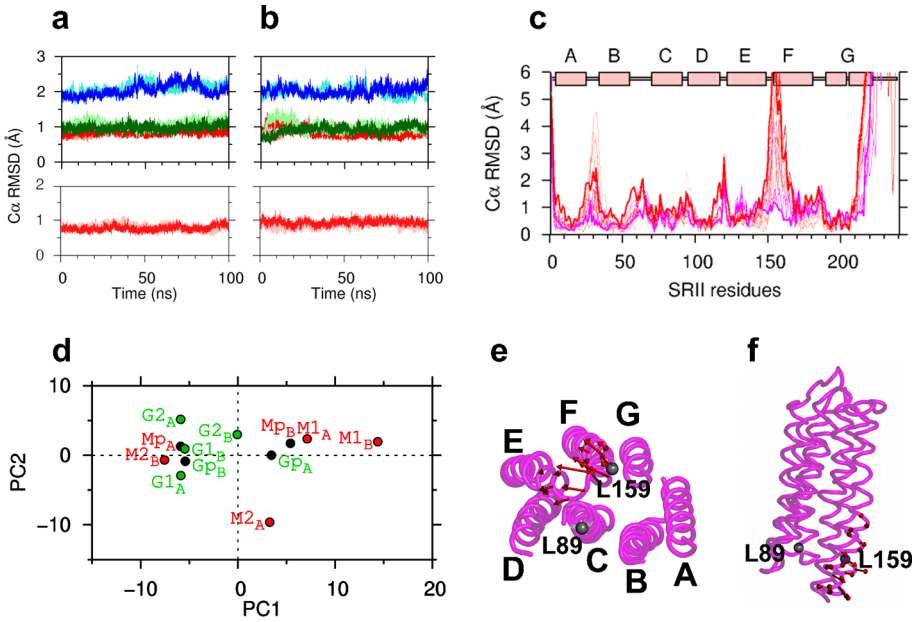

Figure 2. (a and b) Time evolution of the root-mean-square deviation (rmsd) from each crystal structure [PDB entries 1h2s and 2f95 (alternate location B)]: (a) the simulations starting from the ground state structure (G1 and G2) with G1 colored cyan and G2 colored blue for the HAMP domain (rmsd from the NMR structure; PDB entry 2asw with the alignment in ref 29), G1 colored pink and G2 colored red for the transmembrane (TM) region of SRII [$SRII_A$ (top) and $SRII_B$ (bottom); the TM region is defined by residues 4−25, 34−55, 70−91, 95−117, 122−149, 173−181, and 190−204], and G1 colored light green and G2 colored dark green for the TM region of the HtrII dimer (residues 24−43 and 60−81). (b) Simulations starting from the M-intermediate state structure (M1 and M2) with the same coloring scheme as in panel a. (c) Residue profile of the rmsd of the Cα atoms among 16 pairs of the four average structures of $SRII_A$ and $SRII_B$ in G1 and G2 simulations and the four average structures of $SRII_A$ and $SRII_B$ in M1 and M2. (d) Result of the principal component analysis (PCA) using the eight average structures of $SRII_A$ and $SRII_B$ in G1, G2, M1, and M2. The four average structures in Gp and Mp are mapped onto the principal components of the two largest eigenvalues, PC1 (58% contribution) and PC2 (20% contribution). (e) Eigenvector of PC1 plotted on the SRII structure: view from the cytoplasm (left; loops omitted) and view parallel to the membrane (right). The lengths of the vectors are magnified by a factor of 20. The positions of the residues are indicated for L89 (helix C) and L159 (helix F), whose distance was measured by the EPR experiment.[7]

RESULTS AND DISCUSSION

Stability of the Simulation Systems. MD simulations were conducted for the SRII−HtrII complex of *N. pharaonis* with the modeled HAMP domain: simulations G1 and G2 (starting from the ground state structure) and M1 and M2 (from the M-intermediate state structure) are listed in Table 1. The stability of the simulation systems is shown in panels a and b of Figure 2 in terms of the rmsd values of the Cα atoms from the corresponding crystal structures or the NMR structure. The entire complex was stable within the simulation period of 100 ns. The HAMP domain shows a larger rmsd value, but it did not change the structure markedly from the initial structure obtained in the simulation of the isolated HAMP domain[28] whose rmsd value was already ∼2.0 Å from the NMR structure.

Comparison with the Experimental Data: Validation of the Simulation Systems. The structure and position of the modeled HAMP domain in the SRII−HtrII complex were examined in comparison with the information derived from EPR experiments by Steinhoff et al.:[6,24,25,35] inter-residue distances (Figure S2 of the Supporting Information), residue accessibility from the aqueous environment (Figure S3 of the Supporting Information), and residue mobility (Figure S4 of the Supporting Information). Döbber et al.[25] argued on the basis of the EPR experiments that the HAMP domain is in an equilibrium between two conformational states, a highly dynamic (less ordered) state and a more compact (more ordered) state. We concluded from a comparison between the EPR experiments and the simulations (see the Supporting Information) that the simulated HAMP domain structure in the SRII−HtrII complex closely resembles the compact state observed in the EPR data. It is difficult to sample the dynamic state far from the initial structure in a limited simulation time of 100 ns. Therefore, the following discussion is based on the assumption that the HAMP domain stays in the compact state.

Several hydrogen bonds have been reported to be crucial for the SRII−HtrII interactions and the signal transfer.[16−18] The hydrogen bonds important for stabilizing the SRII−HtrII complex are the T189−E43, T189−S62, and Y199−N74 bonds,[17] and the key hydrogen bond for the signal transfer in SRII is the T204−Y174 bond.[18] These bonds were found to be stable in both the ground state simulations (G1 and G2) and the M-state simulations (M1 and M2) (Figure S5 of the Supporting Information). In addition to these stable contacts, local structural changes were observed during the transition from the ground state to the M-state. These changes occurred upon the transfer of a proton from the Schiff base to D75, including the K205−D75, K205−water, D75−water,[22,36] and D75−T79 hydrogen bonds.[18] The formation and cleavage of these hydrogen bonds during the simulations (G1, G2, M1, M2, Gp, and Mp) were found to be consistent with the experiments including the crystal structures (see the Supporting Information for details).

In summary, we observed that the simulation system was stable and maintained the important hydrogen bonds observed in the crystal structures over 100 ns. The structure of the modeled HAMP domain agreed well with the compact state observed in the EPR experiments.

dx.doi.org/10.1021/bi300696b | *Biochemistry* 2012, 51, 5958−5966

Shift of Loop EF and Helix F in SRII. Let us focus on the structural changes in SRII between the ground state and the M-state, observed in the simulations. Figure 2c shows Cα rmsd values between one of the four average structures in the ground state simulations ($SRII_A$ and $SRII_B$ in G1 and G2, respectively) and the four average structures in the M-state simulations. The figure shows that loop EF and the N-terminus of helix F moved greatly, in addition to the large motions in the N- and C-termini, though the rmsd values fluctuated significantly among the average structures. To clarify the structural differences in the average structures, we performed a principal component analysis (PCA) for SRII using the eight average structures obtained in G1, G2, M1, and M2. The results are shown in Figure 2d as the projection of the average structures onto PC1 (58% contribution) and PC2 (20% contribution). Two clusters were clearly separated along PC1: one consisting of the average structures of G1 and G2 and the other of M1 and M2 with the exception of $SRII_B$ in M2.

To illustrate the characteristic coordinates of PC1, separating the M-state from the ground state, we describe the eigenvector of PC1 on the SRII structure in Figure 2e, where loop EF and the cytoplasmic region of helix F move outward. Movements of loop EF and helix F have been observed in various experiments.[6,8,14,15] In Figure 2e, as a reference, the positions of residues L89 (helix C) and L159 (helix F), whose distance was measured by the EPR experiments,[7] are indicated. In the EPR experiments, the distance between the two residues was found to increase, and the outward motion of helix F was proposed as a plausible explanation.[7] This motion is not clearly observed in the M-state crystal structure,[21] but our MD simulations correctly reproduced the experimental observations. The average increase in distance between L89C$_\beta$ and L159C$_\beta$ over the last 50 ns was 1.7 Å. This structural difference in SRII will be discussed again in terms of the interaction between SRII and HtrII.

Rotation of the TM2 Helix in HtrII. Another important motion observed in the experiments is the clockwise rotation (looking from the cytoplasmic side) of the TM2 helix in HtrII along with the transition from the ground state to the M-state.[6,21] To evaluate the rotation of TM2 quantitatively, we devised a side chain Crick angle[28] based on the program TWISTER for the analysis of coiled-coil structures,[37] whose definition is given in the Supporting Information. The side chain Crick angles calculated along the TM2 residues are shown in Figure 3a as well as those of the crystal structure of the M-state.[21] The M-state crystal structure clearly shows a definite clockwise rotation (the negative sign corresponds to clockwise rotation) at the cytoplasmic half of the TM2, though the rotation angle is approximately half of the reported value.[21] The simulation results also indicate clockwise rotations not only in the cytoplasmic half but also in the entire helix with increased magnitudes, though the angles have large deviations. Figure 3b shows the direction of motion together with the residues whose distances have been measured by EPR experiments.[6]

Change in the Overall Orientation of SRII Molecules. A more obvious difference between the ground state and the M-state was seen in the entire complex structure, that is, the orientation of the SRII molecules. As shown in Figure 4a–c, the simulation results in the ground state show that the molecular orientation of the two SRII molecules became more closed than in the ground state crystal structure (Figure 4a), while the orientation became more open than in the M-state crystal

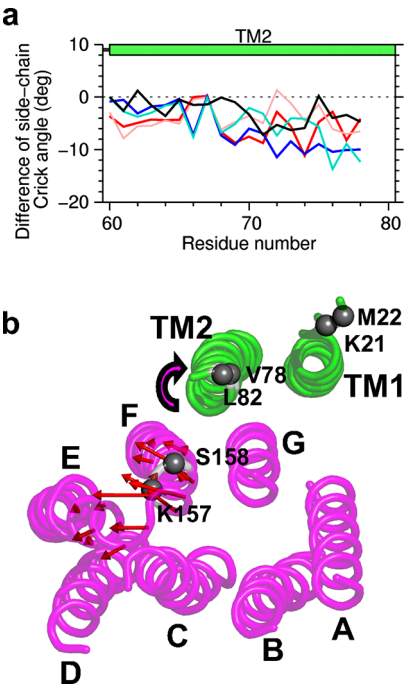

Figure 3. (a) Differences in the side chain Crick angles, defined for the two helices of TM2 in the dimeric HtrII, between the ground state and the M-state: blue for M1 − G1, cyan for M2 − G1, red for M1 − G2, pink for M2 − G2, and black for the difference in the two crystal structures, 2f95 − 1h2s. (b) Molecular view of SRII (magenta) and HtrII (green) from the cytoplasmic side indicating the structural change of SRII from the ground state to the M-state (eigenvector of PC1) and the rotation of TM2 indicated by the side chain Crick angle. The positions of the interface residues between SRII and HtrII, used in the EPR experiments,[6] are also indicated.

structure in the M-state simulations (Figure 4b). It is notable that the two crystal structures have almost the same orientation, as indicated below. The superposition of the two average structures in the ground state and the M-state simulations more clearly indicates the change in the overall orientation of SRII molecules (Figure 4c). To describe this difference more quantitatively, we calculated the orientation angle defined by connecting the centers of the TM regions, $SRII_A$–HtrII dimer–$SRII_B$. Figure 4d (left panel) shows the time evolution of the orientation angle. In G1 and G2, the angle decreased by ∼5° from that of the crystal structure in the ground state, whose angle is 151.2°, immediately after the simulation started. On the other hand, in M1 and M2, the angle increased by less than ∼5° from that of the M-state crystal structure (151.4°), also right after the simulation started. The difference in the orientation angle between the two simulations reached almost 10°.

These quick changes of the orientation angle in a lipid bilayer suggest a possible release from the crystal environment. In the crystal structures, the extracellular end (the turn region between AS1 and AS2 helices, G51 and D52) of HtrII in the adjacent cell is plunged into the cytoplasmic end of HtrII (Figure 4e). The open space at the cytoplasmic end of HtrII is actually filled with long disordered chains that are invisible in the crystal structures: 54 residues (1–22 and 83–114) in the ground state and 104 residues (1–26 and 80–157) in the M-state. These disordered residues may have certain crystal packing effects caused by the proteins in the adjacent cell. We therefore consider that the complex relaxes in the structure

dx.doi.org/10.1021/bi300696b | *Biochemistry* 2012, 51, 5958–5966

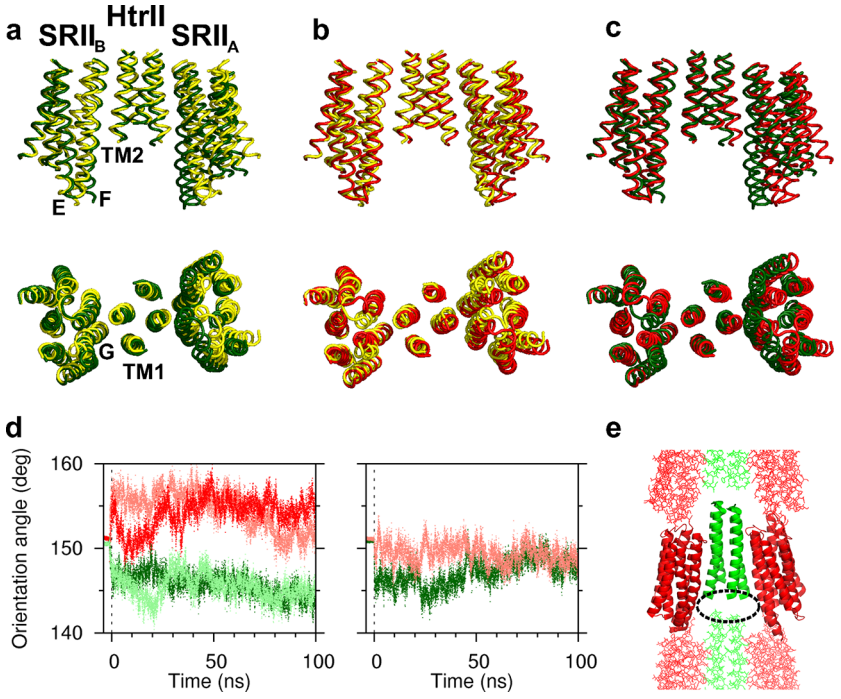

Figure 4. (a) Superposition of the SRII−HtrII complex structures. Average structure of G1 (green) and the crystal structure of the ground state (yellow, PDB entry 1h2s), fitted to their TM domains of SRII$_B$: horizontal view (top) and cytoplasmic view (bottom). The HAMP domain is not shown here for the sake of clarity. (b) Superposition of the average structure of M1 (red) and the crystal structure of the M-state (yellow, PDB entry 2f95). (c) Superposition of the average structures of G1 (green) and M1 (red). (d) Time evolution of the angle of the TM domain defined by connecting the three centers, SRII$_A$−HtrII dimer−SRII$_B$. The left panel shows G1 (light green), G2 (dark green), M1 (pink), and M2 (red). The right panel shows Gp (dark green) and Mp (pink). (e) Crystal packing of the SRII−HtrII complex (PDB entry 1h2s). The cytoplasmic portion of the HAMP domain whose coordinates are missing in the crystal structure (residues 1−22 and 83−114) exists around the region encircled by a dotted line. This region may have a crystal contact with HtrII in the neighboring crystal cell.

without the packing effects when the complex is transferred from the crystal environment to a lipid bilayer.

Interactions between SRII and HtrII. Sudo et al.[19] demonstrated in a binding assay that the interaction between SRII and HtrII is weakened in the M-state compared to the ground state by 25−50-fold. Although these simulations cannot follow such drastic changes, the MD trajectories successfully captured small but significant changes in the interactions. Figure S6 of the Supporting Information shows the number of contacts, both hydrophobic and polar, between SRII and HtrII observed in the simulations; the definition of a contact is given in the legend of Figure S6 of the Supporting Information. Differences were clearly observed in the linker region in HtrII (Figure S6b of the Supporting Information, residues 83−90); the number of contacts in the M-state (1.7 ± 1.5) is almost one-third of the number in the ground state (5.1 ± 3.2). The direction of the change is consistent with the binding experiments, though the magnitude of the change is much smaller than the experimental difference. Among the various contacts, major polar contacts in this region are the G83(HtrII)−N165(SRII) and D85(HtrII)−R162(SRII) contacts in the ground state. In the M-state, the G83−N165 contact was broken but the D85−R162 contact was maintained. Yang et al.[13,14] and Kamada et al.[10] pointed out that G83 is important for signal transduction. Sudo et al.[15] suggested the importance of R162 in the interaction with HtrII. The switched contact, G83−N165, may relate to the function, and the preserved contact, D85−R162, may contribute to stability. These observations thus appear to be consistent with the experimental data.

The weakening of the interaction occurred as a consequence of the opening motion of the entire SRII molecules in the M-state shown in Figure 4. In other words, the opening motion of the entire SRII molecules (more distant from HtrII) dominated the outward shift of helix F (approaching HtrII). We also noticed that the interactions on the extracellular side of TM2 were maintained in the simulations (Figure S6a of the Supporting Information). On the other hand, the interaction with the HAMP domain itself was found to be very weak both in the ground state and in the M-state (Figure S6c of the Supporting Information).

The difference in the interactions between SRII and HtrII is clearly reproduced in the interhelical distance between helix F in SRII and TM2 in HtrII (Figure 5a,b). The smaller distance is in the ground state and the larger distance in the M-state. A close examination of panels a and b of Figure 5 reveals a clear relationship between the interhelical distance and the structural classification of SRII along PC1 shown in Figure 2d (Figure 5c). The correlation coefficient was as large as 0.85. The distance of SRII$_B$ in M2, which shows a ground state-like structure, gives a smaller value of the interhelical distance. We therefore concluded that there is a tight coupling between the structure of SRII and the interactions between SRII and HtrII.

Structural Changes in the Four-Helix Bundle of HtrII. It is difficult to consider that the change in the orientation of SRII shown in Figure 4 occurred as a spontaneous motion of SRII to adapt itself to an optimal orientation in the membrane, because the structural change of the TM region in SRII is small. Therefore, the origin of the orientational change has to be ascribed to another portion of the complex. We consider that

dx.doi.org/10.1021/bi300696b | *Biochemistry* 2012, 51, 5958−5966

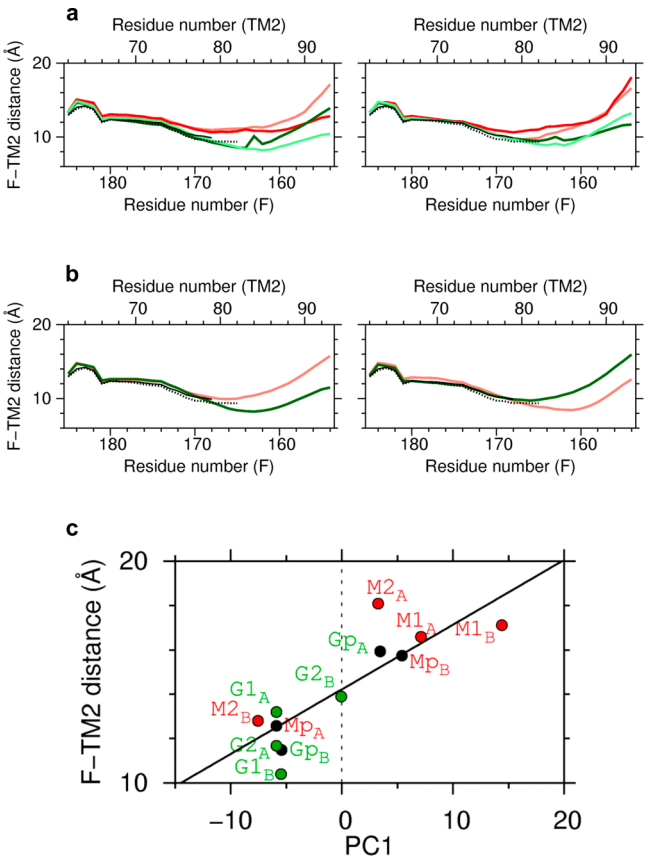

Figure 5. (a) Interhelical distances between helix F and helix TM2 in the simulations with the HAMP domain, defined by the distances between two helical axes, averaged over the last 50 ns of the simulations: G1 (light green), G2 (dark green), M1 (pink), and M2 (red). Left and right panels show the data of the $SRII_B$–$HtrII_B$ and $SRII_A$–$HtrII_A$ pairs, respectively. (b) Interhelical distances in simulations Gp (dark green) and Mp (pink). Distances of the crystal structures of the ground state (black dot) and the M-state (black solid) are also plotted. (c) Correlation between the distances between F-TM2 and PC1 shown in Figure 2. These two factors strongly correlated with a correlation coefficient of 0.85.

the cause is in the four-helix bundle of the HtrII dimer. As shown in Figure 6a, the interhelical distance in the ground state simulations (G1 and G2) between the two TM2 helices in HtrII is shorter by almost 4 Å at residues 70–80 than in the crystal structures. At the same time, the distance between the two TM1 helices is expanded around residues 25–32 compared to that in the crystal structures. On the other hand, the arrangement in the M-state simulations (M1 and M2) maintains the crystal form where the ground state and the M-state take the same structure of HtrII. This means that the four-helix bundle changed the arrangement from orthorhombic (diamond cross section) in the ground state to tetragonal (square cross section) in the M-state. This change in the structure of HtrII, particularly tightly interacting region of residues 70–80, induced the change in the orientation of the SRII molecules.

The structural change of the four-helix bundle can be quantitatively measured by the all atom rmsd values between the structures in G1 and G2 and those in M1 and M2 at each layer of the four-helix bundle (Figure 6b). The rmsd value gradually increases from residue 70 and becomes greater than 5 Å after residue 79. To illustrate the difference, cross sections of the HtrII are shown in Figure 6c–f. It can clearly be seen that there are two types of helix packing, loose packing (the two crystal structures and the M-state simulations, the tetragonal form) and close packing (the ground state simulations, the orthorhombic form).

Influence of the HAMP Domain. Finally, the influence of the HAMP domain is discussed by referring to the MD simulations of the complex without the HAMP domain (the model with only the AS1 helix; Gp and Mp). As for structural stability during the simulation [the rmsd values from the crystal structures (Figure S7 of the Supporting Information)] and the stability of the hydrogen bonds important for stabilization and function [the hydrogen bond distances (Figure S5e,f of the Supporting Information)], the complex without the HAMP domain was stable enough and showed almost no influence of the absence of the HAMP domain. Actually, as shown in Figure S6c of the Supporting Information, almost no direct interaction was observed between SRII and the HAMP domain.

However, when looking at the other details, we found significant differences between Mp and M1 or M2. Figure 2d shows the behavior of loop EF and helix F in SRII in the principal components. Notably, Gp and Mp resulted in a mixed structure; GpB and MpA are in the cluster of the ground state, while GpA and MpB are in the cluster of the M-state. This may suggest a possible role for the HAMP domain in the stability of SRII. This classification precisely matches the distance between helix F in SRII and TM2 in HtrII as shown in Figure 5c; the shorter distance corresponds to the ground state-like structure of SRII and the larger distance to the M-state-like structure. As shown in Figure S8 of the Supporting Information, showing the side chain Crick angle, neither Gp nor Mp exhibited a noticeable rotation of TM2 of HtrII as in G1 and G2, unlike M1 and M2. Figure 4d (right panel) shows the orientation angle of SRII, which clearly indicates that Gp and Mp underwent similar closing motions as in G1 and G2. We noticed in Mp that the closing motion did not occur rapidly, but after more than 50 ns, it eventually attained the same orientation angle as the ground state simulations. The interhelical distance (Figure S9 of the Supporting Information) and the cross section views (Figure S10 of the Supporting Information) of Gp and Mp are also consistent with those of the ground state simulations, or the close packing form.

As shown in these simulation results, the Mp simulation did not exhibit the characteristic motions occurring in the M-state but showed behaviors similar to those in the ground state. Although the influence from the HAMP domain did not appear clearly in Gp, in the case of Mp the existence of the HAMP domain seems to determine the structure, either the M-state-like or the ground state-like structure. What caused these differences in the structures between Mp and M1 or M2?

Here, we try to explain the reason for these differences found in the simulation Mp by focusing on the stability of the four-helix bundle, particularly in the cytoplasmic region. The initial models for simulations Gp and Mp were built simply by extending TM1 and TM2 as α-helices from the crystal structures. The absence of the HAMP domain allowed the elongated helices to remain straight down to the cytoplasmic region. As a result, these models yielded stable interactions in the four-helix bundle almost up to residues 19 in TM1 and 85 in TM2 (for the correspondence of two residues in TM1 and TM2, see Figure S11a of the Supporting Information), which may stabilize the four-helix bundle to assume close packing. On the other hand, the existence of the HAMP domain makes

dx.doi.org/10.1021/bi300696b | *Biochemistry* 2012, 51, 5958–5966

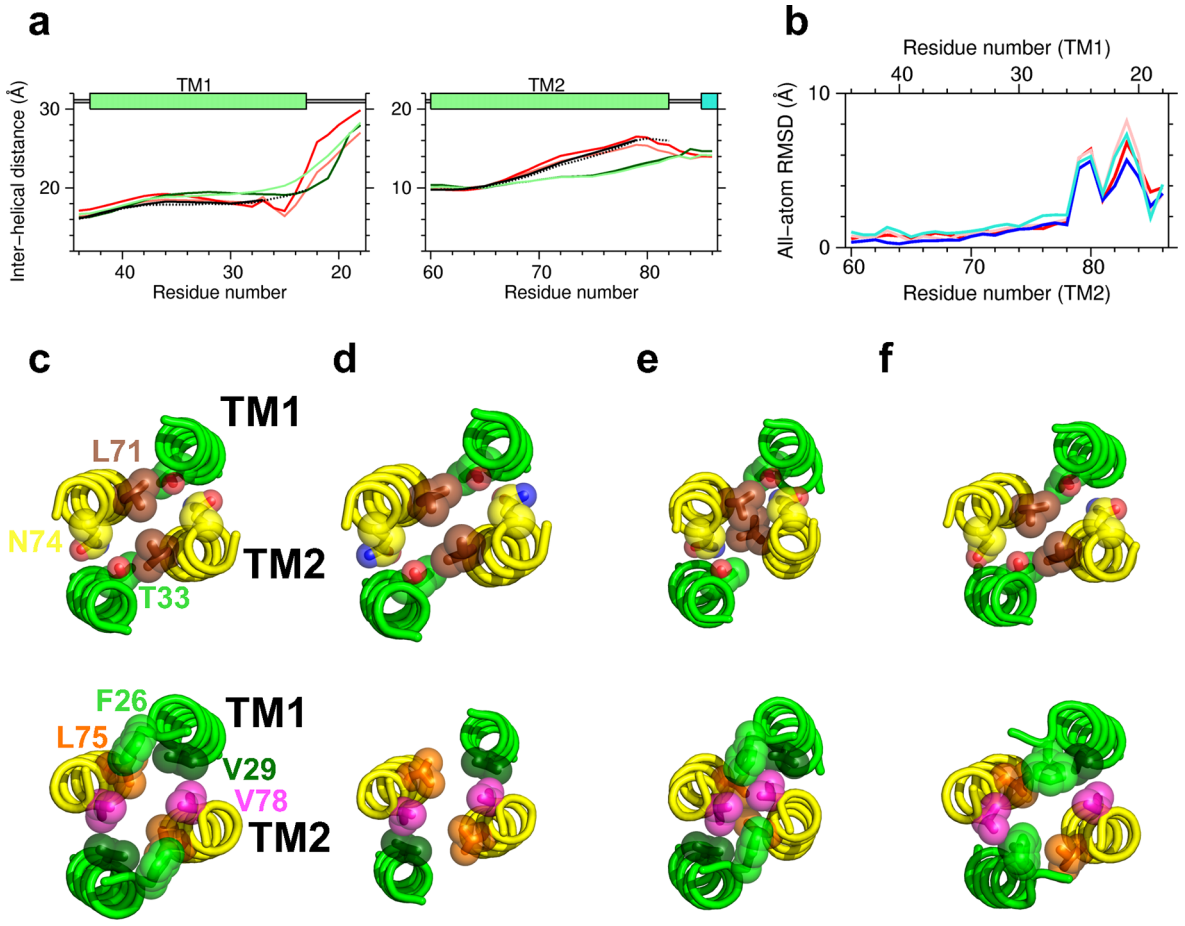

Figure 6. (a) Interhelical distances between two TM1 helices (left) and between two TM2 helices (right) of HtrII, averaged over the last 50 ns: G1 (light green), G2 (dark green), M1 (pink), and M2 (red). The distances of the crystal structures of the ground state (black dot) and the M-intermediate state (black solid) are also plotted. (b) Residue profile of the rmsd for the non-hydrogen atoms of helices TM1 and TM2 among four pairs of the two average structures in G1, G2, M1, and M2 simulations: blue for M1 vs G1, cyan for M2 vs G1, red for M1 vs G2, and pink for M2 vs G2. The superposition was for residues 27−43 and 60−79 in HtrII. Each rmsd value was calculated for residue pairs 60−44, 61−43, ..., 86−18, representing the layers of the HtrII four-helix bundle. (c−f) Hydrophobic side chain packing of the four helices in the HtrII dimer: (c) ground state crystal structure, (d) M-state crystal structure without Phe26, (e) snapshot of G2 at 90 ns, and (f) snapshot of M2 at 80 ns. TM1 and TM2 helices are colored green and yellow, respectively.

TM1 and TM2 bend at around residues 20 and 84, respectively, to avoid a steric clash with the HAMP domain. This bend may make the four-helix bundle marginally stable or allow it to switch between the ground state and M-state structures. In this sense, the extraordinary behavior of simulation Mp can simply be ascribed to the stabilization of the four-helix bundle because of the artificial model without the HAMP domain. Nevertheless, the long relaxation time in Mp (50 ns) shown in Figure 4d (right panel), unlike the rapid relaxation in G1, G2, and Gp, may indicate a significant difference from the ground state structure.

Here, we noticed the important differences in the cytoplasmic region of the four-helix bundle between the ground state and the M-state. The structures of G1 and G2 maintained stable interactions of the bundle up to residues 23 (TM1) and 81 (TM2), in accordance with the crystal structure of the ground state that contains these interactions. On the other hand, simulations M1 and M2 did not achieve stable interactions in the helices after residues 26 (TM1) and 78 (TM2) (see the large values of the root-mean-square fluctuations in Figure S11b of the Supporting Information). These large fluctuations in residues 26−28 coincide with the M-state crystal structure in which the residues involved in these interactions are disordered. Therefore, these differences suggest an importance of the stability of the four-helix bundle in the cytoplasmic region, particularly residues 23−26 in TM1 and 80−82 in TM2, as a determinant of the overall structure of the SRII−HtrII complex.

■ CONCLUDING REMARKS

Here, we summarize the difference between the ground state and the M-state observed in the simulations, following the supposed process of signal transduction. The changes in the hydrogen bond network due to photoexcitation were properly reproduced in the simulations (Figure S5 of the Supporting Information). The structural changes in SRII occurred predominantly in loop EF and helix F (Figure 2). This structural change weakens interactions between SRII and HtrII (Figure S6 of the Supporting Information) through the coupling between the structural changes in SRII and the distance between helix F and helix TM2 (Figure 5c). The weakened interactions triggers the structural transition of the four-helix bundle of HtrII from close packing to loose packing (Figure 6). These structural changes can also be seen in the

dx.doi.org/10.1021/bi300696b | *Biochemistry* 2012, 51, 5958−5966

rotation of TM2 (Figure 3) and in the change in the orientation of the SRII molecules (Figure 4). The structural transition of the four-helix bundle may be related to the destabilization of the stable helix contacts in the cytoplasmic part of HtrII (probably in the region containing residues 26−28 in TM1). When these contacts remain stable, the process converting the ground state to the M-state does not occur [simulation Mp (Figures 4 and 5 and Figures S7−S10 of the Supporting Information)]. These simulation results established the structural basis for the various experimental observations explaining the structural differences between the ground state and the M-intermediate state.

Although we could not observe any significant structural change in the HAMP domain during the M-state simulations, the changes in the packing state of the four-helix bundle will further transmit the signal to the HAMP domain, probably causing some conformational changes in the HAMP domain, as well as in the second HAMP domain that was not included in the simulation model, as proposed in the crystal structure of poly-HAMP domains[38] and in a probe labeling efficiency analysis.[39]

■ ASSOCIATED CONTENT

Supporting Information

Definition of the side chain Crick angle, full description of comparisons between the EPR experiments and the simulations, time evolution of the hydrogen bond distances, time evolution of the total contacts involved in the HtrII−SRII interface, the corresponding residue numbers in the interface region between the TM and the CP domains of HtrII, residue profile of all atom root-mean-square fluctuations, and figures (time evolution of the rmsd, the difference in the side chain Crick angles, the interhelical distances, and the hydrophobic side chain packing of the four-helix bundle of the HtrII dimer) of the simulations without HAMP domains Gp and Mp. This material is available free of charge via the Internet at http://pubs.acs.org.

■ AUTHOR INFORMATION

Corresponding Author

*Address: 1-7-29 Suehiro, Tsurumi, Yokohama 230-0045, Japan. Phone: +81-45-508-7231. Fax: +81-45-508-7367. E-mail: kidera@tsurumi.yokohama-cu.ac.jp.

Present Address

[§]Bioinformatics and Systems Engineering division (BASE), RIKEN, Yokohama 230-0045, Japan.

Funding

This work was supported by Grants-in-Aid for Scientific Research to A.K. from the Ministry of Education, Culture, Sports, Science, and Technology of Japan.

Notes

The authors declare no competing financial interest.

■ ACKNOWLEDGMENTS

The numerical data of the EPR experiments were provided by Prof. Dr. Heinz-Jürgen Steinhoff in Fachbereich Physik, Universität Osnabrück, Osnabrück, Germany. We gratefully acknowledge his kind cooperation. The simulations were performed at the Department of Supramolecular Biology of Yokohama City University and at the Research Center for Computational Science, Okazaki, Japan.

■ ABBREVIATIONS

SRII, sensory rhodopsin II; HtrII, halobacterial transducer of rhodopsin II; MD, molecular dynamics; EPR, electron paramagnetic resonance; HAMP domain, domain found in histidine kinases, adenylyl cyclases, methyl-accepting chemotaxis proteins, and phosphatases; AS1 and AS2, first and the second amphipathic helical segments in the HAMP domain, respectively; TM, transmembrane; CP, cytoplasmic; PDB, Protein Data Bank.

■ REFERENCES

(1) Hoff, W. D., Jung, K. H., and Spudich, J. L. (1997) Molecular mechanism of photosignaling by archaeal sensory rhodopsins. *Annu. Rev. Biophys. Biomol. Struct. 26*, 223−258.

(2) Spudich, J. L., and Luecke, H. (2002) Sensory rhodopsin II: Functional insights from structure. *Curr. Opin. Struct. Biol. 12*, 540−546.

(3) Klare, J. P., Bordignon, E., Engelhard, M., and Steinhoff, H. J. (2004) Sensory rhodopsin II and bacteriorhodopsin: Light activated helix F movement. *Photochem. Photobiol. Sci. 3*, 543−547.

(4) Sasaki, J., and Spudich, J. L. (2008) Signal transfer in haloarchaeal sensory rhodopsin-transducer complexes. *Photochem. Photobiol. 84*, 863−868.

(5) Wegener, A. A., Chizhov, I., Engelhard, M., and Steinhoff, H. J. (2000) Time-resolved detection of transient movement of helix F in spin-labelled *pharaonis* sensory rhodopsin II. *J. Mol. Biol. 301*, 881−891.

(6) Wegener, A. A., Klare, J. P., Engelhard, M., and Steinhoff, H. J. (2001) Structural insights into the early steps of receptor-transducer signal transfer in archaeal phototaxis. *EMBO J. 20*, 5312−5319.

(7) Bordignon, E., Klare, J. P., Holterhues, J., Martell, S., Krasnaberski, A., Engelhard, M., and Steinhoff, H. J. (2007) Analysis of light-induced conformational changes of *Natronomonas pharaonis* sensory rhodopsin II by time resolved electron paramagnetic resonance spectroscopy. *Photochem. Photobiol. 83*, 263−272.

(8) Furutani, Y., Kamada, K., Sudo, Y., Shimono, K., Kamo, N., and Kandori, H. (2005) Structural changes of the complex between *pharaonis* phoborhodopsin and its cognate transducer upon formation of the M photointermediate. *Biochemistry 44*, 2909−2915.

(9) Bergo, V. B., Spudich, E. N., Rothschild, K. J., and Spudich, J. L. (2005) Photoactivation perturbs the membrane-embedded contacts between sensory rhodopsin II and its transducer. *J. Biol. Chem. 280*, 28365−28369.

(10) Kamada, K., Furutani, Y., Sudo, Y., Kamo, N., and Kandori, H. (2006) Temperature-dependent interactions between photoactivated *pharaonis* phoborhodopsin and its transducer. *Biochemistry 45*, 4859−4866.

(11) Kawamura, I., Yoshida, H., Ikeda, Y., Yamaguchi, S., Tuzi, S., Saitô, H., Kamo, N., and Naito, A. (2008) Dynamics change of phoborhodopsin and transducer by activation: Study using D75N mutant of the receptor by site-directed solid-state ^{13}C NMR. *Photochem. Photobiol. 84*, 921−930.

(12) Etzkorn, M., Seidel, K., Li, L., Martell, S., Geyer, M., Engelhard, M., and Baldus, M. (2010) Complex formation and light activation in membrane-embedded sensory rhodopsin II as seen by solid-state NMR spectroscopy. *Structure 18*, 293−300.

(13) Yang, C. S., Sineshchekov, O., Spudich, E. N., and Spudich, J. L. (2004) The Cytoplasmic Membrane-proximal Domain of the HtrII Transducer Interacts with the E-F Loop of Photoactivated *Natronomonas pharaonis* Sensory Rhodopsin II. *J. Biol. Chem. 279*, 42970−42976; (2005) *J. Biol. Chem. 280*, 20915−20916 (erratum).

(14) Yang, C. S., and Spudich, J. L. (2001) Light-induced structural changes occur in the transmembrane helices of the *Natronobacterium pharaonis* HtrII transducer. *Biochemistry 40*, 14207−14214.

(15) Sudo, Y., Iwamoto, M., Shimono, K., and Kamo, N. (2004) Role of Charged Residues of *pharaonis* Phoborhodopsin (Sensory

Rhodopsin II) in Its Interaction with the Transducer Protein. *Biochemistry 43*, 13748−13754.
(16) Sudo, Y., and Spudich, J. L. (2006) Three strategically placed hydrogen-bonding residues convert a proton pump into a sensory receptor. *Proc. Natl. Acad. Sci. U.S.A. 103*, 16129−16134.
(17) Sudo, Y., Yamabi, M., Kato, S., Hasegawa, C., Iwamoto, M., Shimono, K., and Kamo, N. (2006) Importance of specific hydrogen bonds of archaeal rhodopsins for the binding to the transducer protein. *J. Mol. Biol. 357*, 1274−1282.
(18) Sudo, Y., Furutani, Y., Kandori, H., and Spudich, J. L. (2006) Functional importance of the interhelical hydrogen bond between Thr204 and Tyr174 of sensory rhodopsin II and its alteration during the signaling process. *J. Biol. Chem. 281*, 34239−34245.
(19) Sudo, Y., Nishihori, T., Iwamoto, M., Shimono, K., Kojima, C., and Kamo, N. (2008) A long-lived M-like state of phoborhodopsin that mimics the active state. *Biophys. J. 95*, 753−760.
(20) Gordeliy, V. I., Labahn, J., Moukhametzianov, R., Efremov, R., Granzin, J., Schlesinger, R., Büldt, G., Savopol, T., Scheidig, A. J., Klare, J. P., and Engelhard, M. (2002) Molecular basis of transmembrane signalling by sensory rhodopsin II-transducer complex. *Nature 419*, 484−487.
(21) Moukhametzianov, R., Klare, J. P., Efremov, R., Baeken, C., Göppner, A., Labahn, J., Engelhard, M., Büldt, G., and Gordeliy, V. I. (2006) Development of the signal in sensory rhodopsin and its transfer to the cognate transducer. *Nature 440*, 115−119.
(22) Engelhard, M., Scharf, B. E., and Siebert, F. (1996) Protonation changes during the photocycle of sensory rhodopsin II from *Natronobacterium pharaonis*. *FEBS Lett. 395*, 195−198.
(23) Sato, Y., Hata, M., Neya, S., and Hoshino, T. (2005) Computational analysis of the transient movement of helices in sensory rhodopsin II. *Protein Sci. 14*, 183−192.
(24) Bordignon, E., Klare, J. P., Döbber, M., Wegener, A. A., Martell, S., Engelhard, M., and Steinhoff, H. J. (2005) Structural analysis of a HAMP domain: The linker region of the phototransducer in complex with sensory rhodopsin II. *J. Biol. Chem. 280*, 38767−38775.
(25) Döbber, M., Bordignon, E., Klare, J. P., Holterhues, J., Martell, S., Mennes, N., Li, L., Engelhard, M., and Steinhoff, H. J. (2008) Salt-driven equilibrium between two conformations in the HAMP domain from *Natronomonas pharaonis*: The language of signal transfer? *J. Biol. Chem. 283*, 28691−28701.
(26) Sali, A., and Blundell, T. L. (1993) Comparative protein modelling by satisfaction of spatial restraints. *J. Mol. Biol. 234*, 779−815.
(27) Hulko, M., Berndt, F., Gruber, M., Linder, J. U., Truffault, V., Schultz, A., Martin, J., Schultz, J. E., Lupas, A. N., and Coles, M. (2006) The HAMP domain structure implies helix rotation in transmembrane signaling. *Cell 126*, 929−940.
(28) Nishikata, K., Fuchigami, S., Ikeguchi, M., and Kidera, A. (2010) Molecular modeling of the HAMP domain of sensory rhodopsin II transducer from *Natronomonas pharaonis*. *Biophysics 6*, 27−36.
(29) Ikeguchi, M. (2004) Partial rigid-body dynamics in NPT, NPAT and NPγT ensembles for proteins and membranes. *J. Comput. Chem. 25*, 529−541.
(30) MacKerell, A. D., Jr., Bashford, D., Bellott, M., Dunbrack, R. L., Jr., Evanseck, J. D., Field, M. J., Fischer, S., Gao, J., Guo, H., Ha, S., Joseph-McCarthy, D., Kuchnir, L., Kuczera, K., Lau, F. T. K., Mattos, C., Michnick, S., Ngo, T., Nguyen, D. T., Prodhom, B., Reiher, W. E., III, Roux, B., Schlenkrich, M., Smith, J. C., Stote, R., Straub, J., Watanabe, M., Wiorkiewicz-Kuczera, J., Yin, D., and Karplus, M. (1998) All-atom empirical potential for molecular modeling and dynamics studies of proteins. *J. Phys. Chem. B 102*, 3586−3616.
(31) Mackerell, A. D., Jr. (2004) Empirical force fields for biological macromolecules: Overview and issues. *J. Comput. Chem. 25*, 1584−1604.
(32) Feller, S. E., and MacKerell, A. D., Jr. (2000) An improved empirical potential energy function for molecular simulations of phospholipids. *J. Phys. Chem. B 104*, 7510−7515.
(33) Jorgensen, W. L., Chandrasekhar, J., Madura, J. D., Impey, R. W., and Klein, M. L. (1983) Comparison of simple potential functions for simulating liquid water. *J. Chem. Phys. 79*, 926−935.
(34) Essmann, U., Perera, L., Berkowitz, M. L., Darden, T., Lee, H., and Pedersen, L. G. (1995) A smooth particle mesh Ewald method. *J. Chem. Phys. 103*, 8577−8593.
(35) Döbber, M. (2009) Ph.D. Thesis, Universität Osnabrück, Osnabrück, Germany.
(36) Furutani, Y., Iwamoto, M., Shimono, K., Kamo, N., and Kandori, H. (2002) FTIR Spectroscopy of the M photointermediate in *pharaonis* phoborhodopsin. *Biophys. J. 83*, 3482−3489.
(37) Strelkov, S. V., and Burkhard, P. (2002) Analysis of α-helical coiled coils with the program TWISTER reveals a structural mechanism for stutter compensation. *J. Struct. Biol. 137*, 54−64.
(38) Airola, M. V., Watts, K. J., Bilwes, A. M., and Crane, B. R. (2010) Structure of concatenated HAMP domains provides a mechanism for signal transduction. *Structure 18*, 436−448.
(39) Wang, J., Sasaki, J., Tsai, A. L., and Spudich, J. L. (2012) HAMP domain signal relay mechanism in a sensory rhodopsin-transducer complex. *J. Biol. Chem. 287*, 21316−21325.